Dynamic G-quadruplexes on the surface of the human ribosome

Santi Mestre-Fos[1], Petar I. Penev[2], Suttipong Suttapitugsakul[1], Chieri Ito[1], Anton S. Petrov[1], Roger M. Wartell[2], Ronghu Wu[1] and Loren Dean Williams[1,2]†

[1]School of Chemistry and Biochemistry, Georgia Institute of Technology, Atlanta, GA 30332-0400, USA.

[2]School of Biological Sciences, Georgia Institute of Technology, Atlanta, GA 30332-0400, USA

† To whom correspondence may be addressed. Email: loren.williams@chemistry.gatech.edu

Keywords: rRNA, expansion segments, G-tracts, chordates, helicases.

ABSTRACT:

Substantial similarities and profound differences mark ribosomes across phylogeny. The ribosomal core is universal, yet mammalian ribosomes are nearly twice as large as those of prokaryotes. This difference in size is predominantly due to the extension of specific rRNA regions called expansion segments. Here, we characterize expansion segment 7 of the 28S rRNA from *Homo sapiens* by computation, circular dichroism, gel mobility, fluorescent probes, nuclease accessibility, electrophoretic mobility shifts and blotting. Our results indicate that, in a cell-free environment, G-quadruplexes form in human ES7, or 28S rRNA, and in 80S ribosomes or polysomes purified from human cell lines. rRNA G-quadruplex regions are preferentially located on the most surface-exposed regions of the ribosome, near the termini of specific rRNA tentacles in ES7 and ES27. By multiple sequence alignments, we have inferred that G-quadruplex-forming sequences appear to be a general feature of the surfaces of ribosomes of the phylum Chordata. In this study, we also identify the proteins that bind selectively to the rRNA G-quadruplexes, which include several RNA helicases and other RNA remodeling proteins. It is known that G-quadruplexes are contained in telomeres, promoters, and untranslated regions of mRNA but, to our knowledge, they have not been reported to form in ribosomes.

INTRODUCTION

Cytosolic ribosomes of essentially all extant species contain a 'common core'[1] consisting of rRNA and rProteins with universal structure and function. Common core rRNA is reasonably approximated by prokaryotic rRNA; around 90% of prokaryotic rRNA is contained in the common core.

Eukaryotic ribosomes contain additional rRNA and rProteins that form a secondary shell. The rRNA component of the eukaryotic shell contains expansion segments (ESs) that attach to the common core at a handful of specific sites[2-5]. ESs are the most variable rRNA structures over phylogeny, and are known in yeast to play roles in ribosome biogenesis[6] and to bind to chaperone proteins[7-8]. In chordates, ESs form tentacles (Figure 1) that can extend for hundreds of Ångstroms from the ribosomal surface[9]. The lengths of the tentacles are significantly elongated in mammals and reach a zenith in primates and birds.

Here, we observe that human expansion segments 7 and 27 ($ES7_{HS}$ and $ES27_{HS}$) contain rRNA tentacles that form G-quadruplexes *in vitro*. G-quadruplexes are stacked tetrads of guanine bases in tracts separated by short runs of non-specific nucleotides[10]. Focusing on $ES7_{HS}$ we characterize human rRNA by computation, circular dichroism, gel mobility, fluorescent probing, nuclease accessibility, electrophoretic mobility shift assays (EMSA), dot blotting, protein pull-down assays combined with stable isotope labeling with amino acids in cell culture (SILAC) Mass Spectroscopy and Western blotting. G-quadruplexes are observed in isolated human 28S rRNA, and in 80S ribosomes and polysomes.

Multiple Sequence Alignments (MSAs) and database analysis suggests that that G-quadruplex-forming rRNA sequences are found in all chordate species but not in the smaller ribosomes of 'simpler' protists or in ribosomes of prokaryotes. G-quadruplex-forming sequences are located preferentially near termini of rRNA tentacles.

G-quadruplexes have been shown previously to cluster within regulatory RNAs such as 5′ and 3′ untranslated regions of mRNAs[11] and with the first intron[12] but, to our knowledge, they have not been reported to form in ribosomes. Based on our observation of G-quadruplex sequences throughout surface-exposed regions of the ribosomes of chordates (significantly extended in mammals and birds) we hypothesize they recruit specific proteins to the ribosome. The formation of rRNA G-quadruplexes *in vivo* most likely involves the

association/dissociation of specific factors, such that G-quadruplexes are participants in controlled processes.

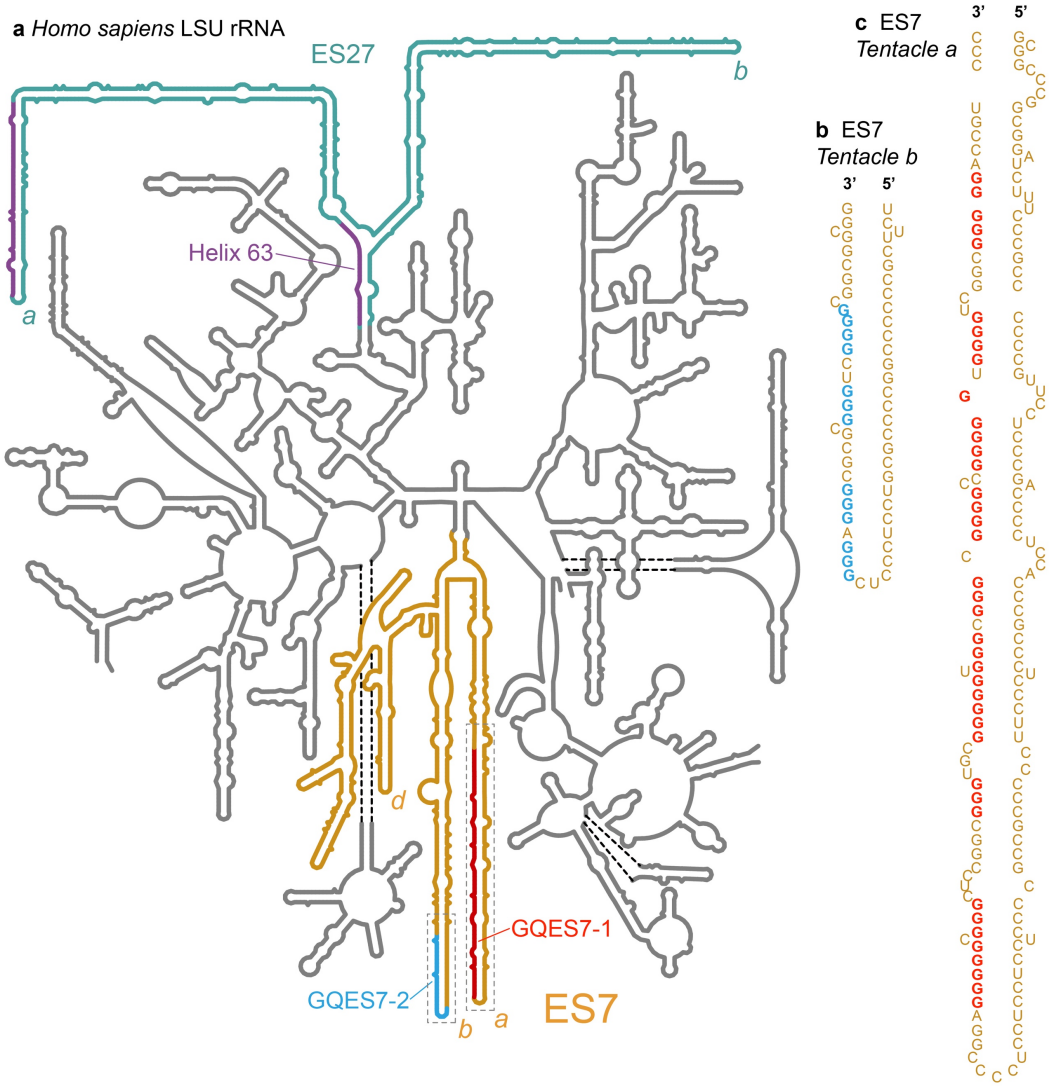

Figure 1. Model secondary structure of the LSU rRNA of *Homo sapiens*. Potential G-quadruplex-forming regions (defined by $G_{\geq 3}N_{1\text{-}7}G_{\geq 3}N_{1\text{-}7}G_{\geq 3}N_{1\text{-}7}G_{\geq 3}$) are highlighted. a) Expansion segment $ES7_{HS}$ is orange. *Tentacles a, b* and *d* of $ES7_{HS}$ are indicated. G-quadruplex-forming regions GQES7-1 (red) and GQES7-2 (cyan) are highlighted. Expansion segment $ES27_{HS}$ is green with purple G-tracts. Helix 63, at the base of $ES27_{HS}$, contains a G-quadruplex motif (purple). *Tentacles a* and *b* of $ES27_{HS}$ are indicated. b) An expanded view of GQES7-2 indicates the sequence. c) An expanded view of GQES7-1.

MATERIALS AND METHODS

$ES7_{HS}$ spans nucleotides 436 to 1311 of the *H. sapiens* LSU rRNA and contains sequences that we call GQES7-1 (nts 583-652) and GQES7-2 (nts 825-853). RNAs

corresponding to $ES7_{HS}$, GQES7-1 and GQES7-2 were synthesized *in vitro* by transcription (HiScribe™ T7 High Yield RNA Synthesis Kit, New England Biolabs). *mt*ES7-1 and *mt*ES7-2 were ordered as RNA oligomers. Baker's yeast tRNAs were purchased from Roche. RNA purity was monitored by 8 M Urea 5% acrylamide gel in TBE buffer. Complete sequences of $ES7_{HS}$, GQES7-1, GQES7-2, *mt*ES7-1 and *mt*ES7-2 are contained in Table S.1.

HEK293T 28S rRNA extraction and purification. HEK293T cells were grown to 60% confluency after which total RNA was extracted with TRI Reagent® (Sigma-Aldrich). 28S rRNA was extracted from an agarose gel by running the rRNA into wells in the center of the gel, where the rRNA was extracted with a pipette. The rRNA was precipitated in 5 M ammonium acetate-acetic Acid, pH 7.5 with excess ethanol. 28S rRNA purity was monitored on 1% agarose gels (Figure S.1).

Thioflavin T (ThT) fluorescence. RNAs were prepared at a final concentration of 0.6 μM (strand) and annealed in 150 mM KCl, 10 mM Tris-HCl, pH 7.5, 2 μM ThT by cooling from 90°C to 25°C at 1°/min. RNAs were incubated at 4°C for 10 min and were loaded onto a Corning® 384 Well Flat Clear Bottom Microplate. Fluorescence from 300-700 nm, exciting at 440 nm were acquired on a BioTek Synergy™ H4 Hybrid plate reader. When appropriate, pyridostatin (PDS) was added to the desired concentration after the RNA was annealed.

Circular dichroism. RNA at 2 μM (strand) in 50 mM KCl and 10 mM Tris-HCl (pH 7.5) was annealed as described above. CD spectra were acquired at 20 °C on a Jasco J-810 spectropolarimeter using 1 mm cuvettes. Data from 200-320 nm was acquired at a rate of 100 nm/min with 1 sec response, a bandwidth of 5 nm, and averaged over three measurements. The buffer spectrum was subtracted. Smoothing was performed with Igor Pro. The observed ellipticity (θ, mdeg) was normalized[13] using the expression $\Delta\varepsilon = \theta/(32{,}980 \times c \times l)$, where c is the molar strand concentration of the RNA and l is the path length of the cuvette in centimeters.

Ion-dependent electrophoresis. Aliquots of RNAs at 1 μM (strand) were annealed in the presence of either Na^+ or Li^+ or K^+ at various concentrations (50 mM, 100 mM, 250 mM) in 10 mM Tris-HCl, pH 7.5. Samples were mixed with glycerol (50%) and resolved on 5% native acrylamide gels, which were stained for 15 min in 0.5 μM ThT and imaged on an Azure imager c400 (Azure Biosystems).

EMSAs. The anti-G-quadruplex BG4 antibody was purchased from Absolute Antibody (Catalog #: Ab00174-1.1). GQES7-1 (3 μM) rRNA or the negative control *mt*ES7-1 RNA were annealed in 20 mM Hepes-Tris, pH 7.5, 50 mM KCl. GQES7-1 rRNA or *mt*ES7-1 RNA were combined with various concentrations of BG4 at a final RNA concentration of 1 μM RNA (strand). RNA-protein mixtures were incubated at room temperature for 20 min in 50 mM KCl. RNA-protein interactions were analyzed by 5% native-PAGE. Gels were visualized following a dual fluorescent dye protocol[14] with a Azure imager c400 (Azure Biosystems).

rRNA - BG4 antibody dot blotting. RNAs were annealed in the presence of 50 mM KCl and were diluted 1x, 2x and 4x. GQES7-1, GQES7-2, *mt*ES7-2, tRNA: 3.2 μM, 1.6 μM 0.8 μM. $ES7_{HS}$: 1.4 μM, 0.7 μM, 0.35 μM. 28S rRNA: 55 nM, 27.5 nM, 13.7 nM. RNAs were loaded onto nitrocellulose membranes and dried at room temperature for 30 min. RNAs were cross-linked with the membrane in a GS Gene Linker™ UV Chamber (Bio Rad). The membranes were blocked for 1 h at room temperature. BG4 antibody was added (1:2,000 dilution) and incubated with gentle rocking for sixty min at room temperature. The membrane was washed for ten min twice with 1X TBST and incubated for sixty min with an appropriate fluorescent secondary antibody anti-mouse (1:10,000 dilution) (Biotium, #20065-1). The membrane was washed for ten min twice with 1X TBST and was imaged on a Li-Cor Odyssey Blot Imager. Intact 80S ribosomes and polysomes (purified from HEK293) were incubated at room temperature for 15 min in the presence of 50 mM KCl with or without 10 μM PDS. Ribosomes or polysomes were added iteratively in 30-min intervals to the same site on a nitrocellulose membrane (0.9 μg, 2.7 μg, 4.5 μg). The membrane was then treated as described above. BG4 was added to a final dilution of 1:1,000 and the secondary antibody was added to a final dilution of 1:5,000.

Mung bean nuclease (MBN) probing. $ES7_{HS}$ and tRNA were prepared at 100 ng/μL and annealed in the presence/absence of 100 mM KCl, 15 mM Tris-HCl (pH 7.5) by cooling from 90°C to 25°C, at 1°/min. PDS was added to the annealed RNA to a final concentration of 2 μM. One unit of MBN was added per μg of RNA and samples were incubated at 30°C for 30 min. SDS was added to a final concentration of 0.01% to denature the nuclease and RNA was purified by ethanol precipitation. The extent of RNA cleavage was determined on an 8 M urea 5% acrylamide (19:1 acrylamide/bisacrylamide) gel stained with ethidium bromide.

ES7 secondary structures. Secondary structures of human and *D. melanogaster* ES7 were obtained from RiboVision[15]**.** Nucleotides of G-quadruplex regions in *P. troglodytes*, *M. musculus* and *G. gallus* (Table 1) were numbered as in Bernier[1], subtracting the nucleotides from the 5.8S rRNA.

Phylogeny and Multiple Sequence Alignments. The SEREB MSA[1] was used as a seed to align additional eukaryotic ES7 sequences to increase the density of eukaryotic species in the MSA. The 28S rRNA sequences in the SEREB MSA were used to search[16] the NCBI databases[17] for LSU rRNA sequences. The SEREB database has sequences from 10 chordate species; seven additional chordate species from 7 new orders were added to the ES7 *tentacle a* MSA (Figure 7, Table S.3). Sequences without intact ES7 *tentacle a* were excluded. Sequences with partial 28S rRNA were marked as partial. Sequences inferred from genomic scaffolds were marked as predicted (Table S.3). The extended database was queried for G-quadruplex-forming sequences.

Sequences were incorporated into the SEREB-seeded MSA using MAFFT[18] and adjusted manually using BioEdit[19]. Manual adjustments incorporated information from available secondary structures. In some cases, the positions of G-tracts in sequences with large gaps relative to *H. sapiens* are not fully determined, as they can be aligned equally well with flanking G-tracts in the MSA. Alignment visualization was done with Jalview[20]. The phylogenetic tree and the timeline of clade development were inferred from TimeTree[21].

Analysis of the entire LSU was performed on SEREB sequences, which are highly curated and always complete. This procedure ensured that negative results indicate absence of G-quadruplex-forming sequences from intact rRNAs rather than absence from rRNA fragments that lack the appropriate regions. G-quadruplex-forming sequences are not detected in any of the 20 non-chordate members of the SEREB database.

SILAC. HEK293T cells were cultured in SILAC media - “heavy” or “light” Dulbecco's Miodified Eagle Media (DMEM) (Thermo Scientific) supplemented with 10% dialyzed fetal bovine serum (FBS) (Corning) and 1% penicillin-streptomycin solution (Sigma) in a humidified incubator at 37 ˚C with 5% carbon dioxide. The heavy media contained 0.798 mM L-lysine ($^{13}C_6$ and $^{15}N_2$, Cambridge Isotope Laboratories) and 0.398 mM L-arginine ($^{13}C_6$, Cambridge Isotope Laboratories). The light media had the same concentrations of normal lysine and arginine (Sigma). Media were supplemented with 0.2 mg/mL proline (Sigma) to

prevent arginine-to-proline conversion. Heavy and light cells were grown for at least six generations. Once the confluency reached 80%, cells were harvested by scraping, washed twice with ice-cold PBS (Sigma), lysed in a buffer containing 10 mM HEPES pH=7.4, 200 mM potassium chloride, 1% Triton X-100, 10 mM magnesium chloride (all from Sigma) and 1 pill/10 mL cOmplete ULTRA tablet protease inhibitor (Roche), and incubated on an end-over-end shaker at 4 ^{o}C for 1 hour. Lysates were centrifuged at 25,830 g at 4 ^{o}C for 10 minutes, and the supernatants were collected and kept on ice.

Ten μg of GQES7-1-Biotin RNA was annealed as described above in the presence of 10 mM Tris-HCl, pH 7.5, and 100 mM KCl. Twenty μL of magnetic streptavidin-coated beads (GE Healthcare) were washed with Lysis buffer (10 mM HEPES, pH 7.4, 200 mM KCl, 1% Triton X-100, 10 mM $MgCl_2$, protease inhibitors). Annealed RNA was then added to the washed beads and incubated at 4^{o}C for 30 min with gentle shaking. For control experiments, no RNA was added. SILAC cell lysates were incubated with 0.5 mg *E. coli* tRNA per 1 mg protein at 4^{o}C for 30 min with gentle shaking. "RNA+Beads" and control "Beads Only" samples were transferred into the SILAC cell lysates: "RNA+Beads" were added to the Heavy cell lysate and "Beads Only" was added to "Light" HEK293T cell lysate. As a replicate, "RNA+Beads" was added "Light" cell lysate and "Beads Only" was added to "Heavy" cell lysate. 200 U/mL of RNasin was added and the lysates were incubated at 4 ^{o}C for 2 hrs with gentle shaking. Samples were centrifuged, the supernatant was discarded, and the pelleted beads were washed with lysis buffer with increasing KCl concentrations (0.4 M, 0.8 M, 1.6 M). After the three washes, 100 μL of the elution buffer (100 mM Tris-HCl, pH 7.4, 1% SDS, 100 mM DTT) was added to one of the two samples and then combined with the beads of the corresponding sample. "RNA+Beads" in "Heavy" lysates were combined with "Beads Only" in "Light" lysates and "RNA+Beads" in "Light" lysates were combined with "Beads Only" in "Heavy" lysates. The combined samples were boiled and then briefly centrifuged. Beads were discarded and samples were analyzed with an online LC-MS system.

Mass spectrometry analyses. Eluted proteins were diluted 10 times with 50 mM HEPES pH=7.4 and were alkylated with 28 mM iodoacetamide (Sigma) for 30 minutes at room temperature in the dark. Proteins were precipitated by methanol-chloroform, and the pellets were resuspended in digestion buffer containing 50 mM HEPES pH=8.8, 1.6 M urea,

and 5% acetonitrile (ACN) (all from Sigma). After digestion with sequencing-grade modified trypsin (Promega) at 37 ˚C for 16 hours, reactions were quenched with 1% trifluoroacetic acid (TFA, Fisher Scientific) and purified with StageTip. Peptides were dissolved in 10 µL 5% ACN and 4% FA solution, and 1 µL was loaded to a Dionex UltiMate 3000 UHPLC system (Thermo Fisher Scientific) with a microcapillary column packed in-house with C18 beads (Magic C18AQ, 5 mm, 200 Å, 100 mm 16 cm). A 110-minute gradient of 3-22% ACN containing 0.125% FA was used. The peptides were detected with an LTQ Orbitrap Elite Hybrid Mass Spectrometer (Thermo Fisher Scientific) controlled by Xcalibur software (version 3.0.63). MS/MS analysis was performed with a data-dependent Top20 method. For each cycle, a full MS scan in the Orbitrap with the automatic gain control (AGC) target of 10^6 and the resolution of 60,000 at 400 m/z was followed by up to 20 MS/MS scans in the LTQ for the most intense ions. Selected ions were excluded from further sequencing for 90 seconds. Ions with singly or unassigned charge were not sequenced. Maximum ion accumulation times were 1,000 ms for each full MS scan and 50 ms for each MS/MS scans. The spectra were searched against a human protein database downloaded from UniProt using the SEQUEST algorithm (version 28)[22]. The following parameters were used: 20 ppm precursor mass tolerance; 1.0 Da fragment ion mass tolerance; trypsin digestion; maximum of 3 missed cleavages; differential modifications for methionine oxidation (+15.9949 Da), heavy lysine (+8.0142 Da), and heavy arginine (+6.0201 Da); fixed modification for cysteine carbamidomethylation (+57.0215 Da). The false discovery rates (FDR) were evaluated and controlled by the target-decoy method. Linear discriminant analysis (LDA) was used to filtered the peptides to <1% FDR based on parameters such as XCorr, differential sequence ΔC_n, and precursor mass error. An additional filter was used to control the protein FDR to <1%. For SILAC quantification, the S/N ratios of both heavy and light peptides must be greater than 3. Otherwise, one of the two versions of the peptides (heavy or light) must have the S/N ratio greater than 10. Other peptides that did not pass these criteria were removed. The final protein ratio was calculated from the median value of the peptides from each parent protein. The raw files are publicly accessible at http://www.peptideatlas.org/PASS/PASS01260, Username: PASS01260, Password: TL3854zn.

Western Blotting. Samples were electrophoresed on 12% SDS-PAGE gels and transferred to a nitrocellulose membrane overnight. Membranes were blocked for 1 hour at room temperature with gentle shaking and then incubated for another hour with primary antibodies: 1:200 dilution of FIP1 (mouse monoclonal, sc-398392), DDX3 (mouse monoclonal, sc-81247), FUS (mouse monoclonal, sc-47711), or hnRNP H (mouse monoclonal, sc-32310). Antibodies were obtained from Santa Cruz Biotechnology. Membranes were washed three times with 1X TBST and secondary antibody CF680 goat anti-mouse IgG (H+L) (Biotium, 20065) was added (1:5,000 dilution). Membranes were washed three times with 1X TBST and imaged on a Li-Cor Odyssey Blot Imager.

RESULTS

ES7 and ES27 are the only regions within the human LSU that contain putative G-quadruplex sequences. The propensity of an RNA to form G-quadruplexes can be roughly predicted by numbers and lengths of guanine tracts and the lengths and compositions of loops. The program QGRS Mapper[23] provides "G-scores", which quantitate this propensity. We have identified ES7 and ES27 as the only human LSU rRNA regions containing sequences reasonably capable of forming these secondary structures. Our computational results suggest that G-quadruplexes can form in the guanine-rich strands at the termini of the longest rRNA tentacles of these two ESs. In tentacles *a* and *b* of $ES7_{HS}$, two regions, here named GQES7-1 and GQES7-2 (Figure 1), meet the G-quadruplex consensus ($G_{\geq 3}N_{1\text{-}7}G_{\geq 3}N_{1\text{-}7}G_{\geq 3}N_{1\text{-}7}G_{\geq 3}$). The G-scores of GQES7-1 and GQES7-2 are in the range of well-established RNA G-quadruplexes.

The sequence 5' GGGGCCGGGGGUGGGGUCGGCGGGG 3' (nts 623-647, within GQES7-1, Figure 1, Table 1) gives a G-score of 60. The sequence 5' GGGUGCGGGGGUGGGCGGG 3' (nts 603-621, also within GQES7-1) gives a G-score of 40. The sequence 5' GGGAGGGCGCGCGGGUCGGGG 3' (nts 829-849 within GQES7-2, Figure 1, Table 1) gives a G-score of 38. The difference between the G-scores of GQES7-1 and GQES7-2 suggests more stable and/or more extensive G-quadruplex formation in GQES7-1 than in GQES7-2. A greater propensity of GQES7-1 over GQES7-2 for G-quadruplex formation is seen in all experiments below.

Table 1. G-quadruplex-forming regions within ES7 and ES27 rRNA

ES7		**Nucleotides**
tentacle a		
Homo sapiens	**GGGGG**C**GGG**CUCCGGC**GGG**UGC**GGGGG**U**GGG**C**GGG**C**GGGG**CC**GGGGG**U**GGGG**UCGGC**GGGGG**	587-648
Pan troglodytes	**GGGGG**C**GGG**CUCCGGC**GGG**UGC**GGGGG**U**GGG**C**GGG**C**GGGG**CC**GGGGG**U**GGGG**UCGGC**GGGGG**	583-644
Mus musculus	**GGG**C**GGGG**CC**GGGGG**U**GGGG**UCGGC**GGGGG**	627-656
Gallus gallus	**GGGG**C**GGGG**C**GGG**CCCA**GGGGGGG**C**GGG**C**GGG**CC**GGGG**	557-594
tentacle b		
Homo sapiens	**GGG**A**GGG**CGCGC**GGG**UC**GGGG**	829-849
Pan troglodytes	**GGG**A**GGG**CGCGC**GGG**UC**GGGG**	816-836
tentacle d		
Mus musculus	**GGG**C**GGG**CGU**GGGGG**U**GGGGG**CC**GGG**	907-932
Gallus gallus	**GGGG**CGC**GGGGG**C**GGGGGGGG**UC**GGG**	933-958
ES27		
tentacle a		
Homo sapiens	**GGGGG**AGCGCCGCGU**GGGGG**CGGCGGC**GGGGGG**AGAA**GGG**UC**GGGG**CGGCA**GGGG**	3095-3149
tentacle b		
Homo sapiens	**GGGGG**C**GGGG**AGCGGUC**GGG**CGGCGGCGGUCGGC**GGG**CGGC**GGGG**C**GGGG**[a]	3373-3422
helix 63		
Homo sapiens	**GGG**CU**GGG**UCGGUC**GGG**CU**GGGG**	2896-2918

a. This sequence falls outside the $G_{\geq 3}N_{1\text{-}7}G_{\geq 3}N_{1\text{-}7}G_{\geq 3}N_{1\text{-}7}G_{\geq 3}$ motif

As a positive control for our computations and experiments, we used the ADAM10 G-quadruplex. This stable and well-characterized G-quadruplex-forming RNA, found in the 5'-UTR of the mRNA of ADAM10 metalloprotease[24], gives a G-score of 42. As negative controls, we used two mutant RNA oligomers (*mt*ES7-1 and *mt*ES7-2) that are analogous to GQES7-1 and GQES7-2 in composition and length, with disrupted G-tracts (Table S.1). Neither gives a G-score.

Near the terminus of human ES27 ($ES27_{HS}$, Figure 1, Table 1), the sequence 5' GGGGAGAAGGGUCGGGGCGGCAGGG 3' (nts 3124-3148, *tentacle a*) gives a G-score of 40. $ES27_{HS}$ also contains a putative G-quadruplex-forming region in Helix 63 near the junction of two tentacles. In this study, we focused only $ES7_{HS}$. However, based on the high correlation

of G-scores and our experimental observation of G-quadruplexes within $ES7_{HS}$, we expect G-quadruplexes to also form in $ES27_{HS}$.

G-quadruplex formation within GQES7-1, GQES7-2, and intact $ES7_{HS}$. We investigated the ability of the two regions within $ES7_{HS}$ (GQES7-1 and GQES7-2, Figure 1) to form G-quadruplexes *in vitro* by several methods.

ThT fluorescence. ThT is known to yield intense fluorescence at 487 nm upon association with G-quadruplexes[25-26]. ThT results here suggest formation of G-quadruplexes in GQES7-1, GQES7-2 and intact $ES7_{HS}$ in the presence of K^+, the monovalent ion thought to stabilize G-quadruplexes (Figure 2a). The signal for GQES7-2 is attenuated compared to that of GQES7-1. This difference, which suggests less stable G-quadruplexes and/or less extensive G-quadruplex formation of GQES7-2, is consistent with the computed propensity and is observed here in a variety of assays. The formation of G-quadruplexes by GQES7-1, GQES7-2 and intact $ES7_{HS}$ is also supported by competition assays with pyridostatin (PDS) (Figure S.2). PDS is a G-quadruplex stabilizer and a ThT competitor with a greater affinity than ThT for G-quadruplexes[27]. In this series of experiments ADAM10 was used as a positive control and *mt*ES7-1, *mt*ES7-2 and tRNA were used as negative controls.

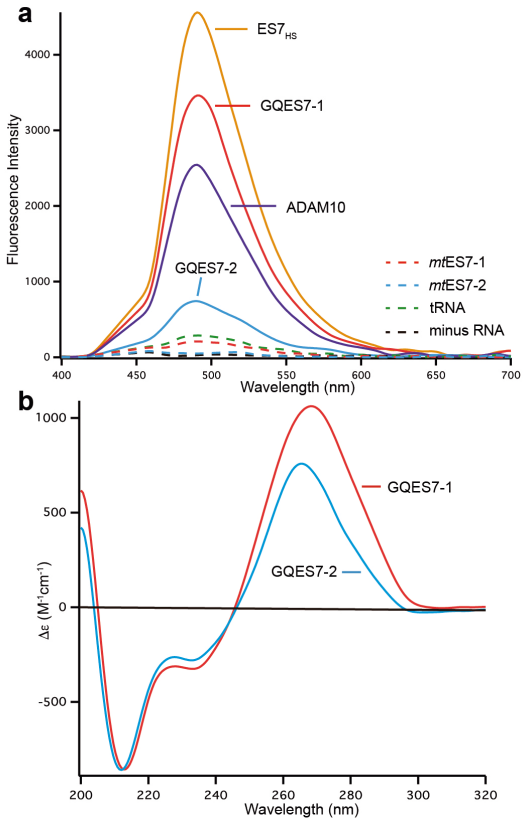

Figure 2. Formation of G-quadruplexes in GQES7-1, GQES7-2, and $ES7_{HS}$. a) Fluorescence emission of ThT in the presence of $ES7_{HS}$, GQES7-1, GQES7-2, or ADAM10. Negative controls (dashed) are tRNA, *mt*ES7-1, *mt*ES7-2 and minus RNA. b) CD spectra of GQES7-1 and GQES7-2.

Circular dichroism. CD has been used widely to study RNA and DNA G-quadruplexes. Our CD spectra of GQES7-1 and GQES7-2 are consistent with formation of parallel G-quadruplexes based on a characteristic peak at 260 nm and a trough at 240 nm[28-32] (Figure 2b).

G-quadruplexes are thought to be more stable in K^+ than in Li^+ or Na^+[33]. The intensity of the 260 nm peak of GQES7-1 is attenuated by about 15% when the monovalent cation is switched from K^+ to Na^+ or Li^+ (not shown).

Gel staining. ThT staining of GQES7-1 and GQES7-2 after native gel electrophoresis in the presence of Na^+ or Li^+ or K^+ is in agreement with the CD data (Figure 3a and 3b). The RNAs are expected to fluoresce within the gel only upon formation of G-quadruplexes. GQES7-1 and GQES7-2 fluoresce more intensely in the presence of K^+ than in Na^+ or Li^+. Consistent with computation, ThT fluorescence in solution, and CD spectroscopy, GQES7-1 forms more extensive G-quadruplexes than GQES7-2 in the gel staining experiments.

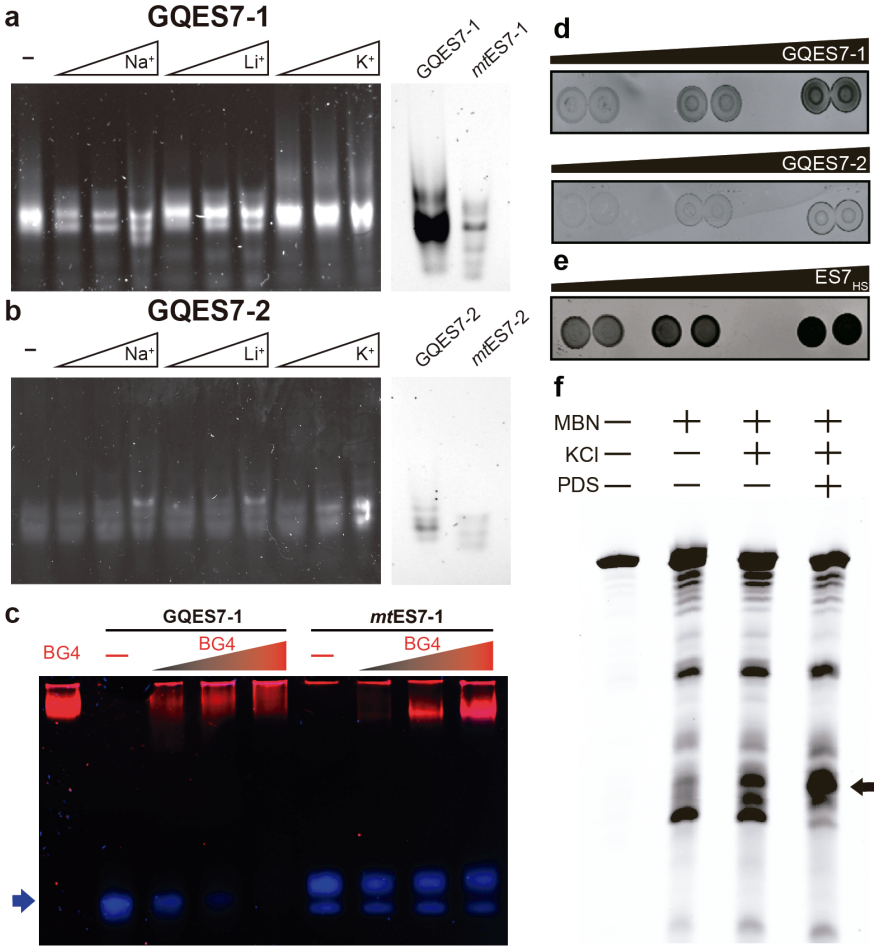

Figure 3. The effect of monovalent ion type on G-quadruplex formation. Shown here are a) GQES7-1 and b) GQES7-2 RNAs with varying concentrations of Na^+, Li^+, and K^+ (50, 100, 250 mM), resolved on a native gel stained with ThT. The mutants *mt*ES7-1 and *mt*ES7-2 do not fluoresce when stained with ThT, indicating the lack of G-quadruplex formation in these RNAs (gels on the right). c) EMSA of the BG4 antibody with GQES7-1 and its mutant *mt*ES7-1, visualized on a native gel. GQES7-1 and *mt*ES7-1 RNAs were loaded at a constant strand concentration with increasing concentrations of BG4 antibody. The RNA (arrow) is blue and the protein is red. d) Dot blots with the BG4 G-quadruplex antibody with a) GQES7-1 or GQES7-2 (0.8 μM, 1.6 μM, 3.2 μM) and e) intact $ES7_{HS}$ (0.35 μM, 0.7 μM, 1.4 μM). f) d) $ES7_{HS}$ cleavage by mung bean nuclease. ES7 was annealed with or without KCl and with or without PDS. The black arrow indicates cleaved rRNA.

Antibody binding. BG4 is an antibody developed by Balasubramanian and coworkers[34-35] that binds to a variety of G-quadruplex types but not to other nucleic acids such as RNA hairpins, single-stranded or double-stranded DNA. Here, an EMSA was performed with BG4 to test for G-quadruplex formation in GQES7-1 (Figure 3c). BG4 was also used for dot blotting experiments with GQES7-1, GQES7-2, and intact $ES7_{HS}$ (Figure 3d and

3e). We observe binding of GQES7-1, GQES7-2, and intact $ES7_{HS}$ with BG4. As expected from the results above, GQES7-1 binds more tightly than GQES7-2 to BG4, which is close to background levels (Figure S.3).

Mung bean nuclease cleavage. RNA G-quadruplexes have been studied primarily in the context of mRNA, which is single-stranded. However, the regions of 28S rRNA capable of forming G-quadruplexes are opposed by complementary C-rich strands (Figure 1). In rRNA, upon G-quadruplex formation, the C-rich strand would be forced to dissociate to a single strand. To confirm this model, we examined cleavage of $ES7_{HS}$ by mung bean nuclease (MBN) (Figure 3f), which preferentially cleaves single-stranded RNA and DNA. The results here show that MBN cleaves $ES7_{HS}$ under G-quadruplex stabilizing conditions to a greater extent than under conditions that destabilize G-quadruplexes (Figure 3f). Addition of K^+ increases the extent of cleavage and addition of PDS to K^+ further increases the extent of cleavage. The simplest interpretation of these results is that $ES7_{HS}$ is dynamic and can exist as a mixture of duplex and G-quadruplex forms. As a negative control, extent of MBN hydrolysis of tRNA did not increase upon addition of K^+ and/or PDS (Figure S.4).

G-quadruplex formation in 28S rRNA or 80S human ribosomes or polysomes.

The experiments presented above confirmed that the sequences within human rRNA ES7 of the 28S rRNA are capable of forming G-quadruplexes. We have investigated whether the 28S rRNA obtained from cells could form G-quadruplexes when this RNA is rProtein-free or assembled in ribosomes.

The 28S rRNA was extracted from HEK293T cells and dot blotting was performed with BG4 (Figure 4a). The results indicate that 28S rRNA forms G-quadruplexes *in vitro*. To confirm that the 28S rRNA is capable of forming G-quadruplexes when assembled in the intact ribosome, dot blotting was also performed with purified 80S human ribosomes and polysomes (Figure 4b).

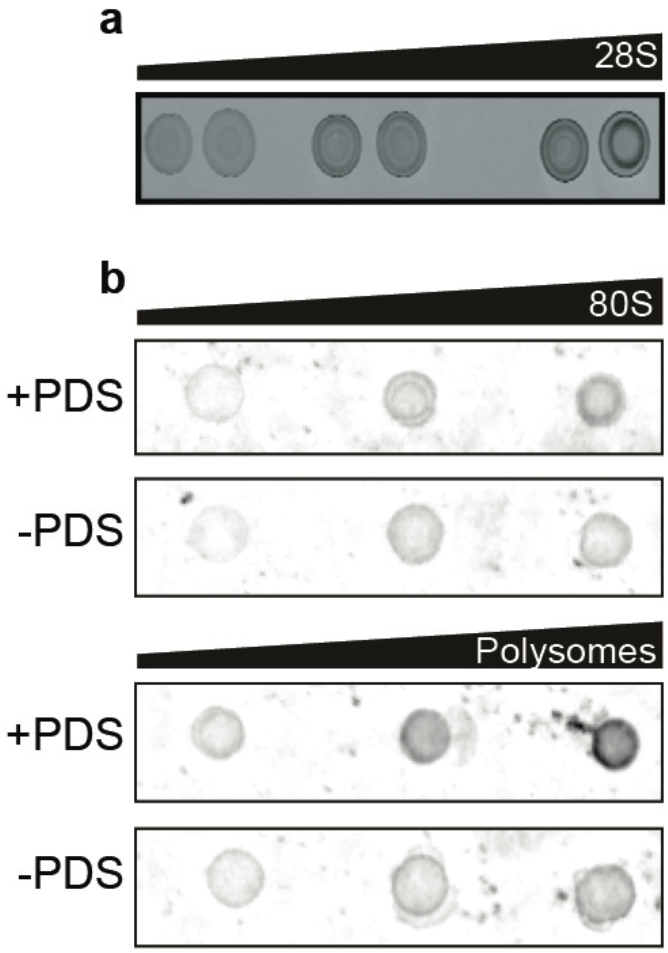

Figure 4. Dot blots performed with the BG4 antibody on a) the 28S rRNA extracted from HEK293T cells and on b) human 80S ribosomes and polysomes purified from HEK293 cells. All samples were incubated in the presence of 50mM KCl and ribosomes and polysomes were further analyzed with or without 10 μM PDS, which stabilizes G-quadruplexes. Samples were loaded onto the membrane in increasing amounts from left to right.

The results show that the BG4 antibody selectively binds to intact human ribosomes and polysomes in a concentration-dependent manner. PDS enhances binding of the antibody, as expected. The more extensive binding of the antibody to polysomes than to monomer

ribosomes suggests the possibility of formation intermolecular of G-quadruplexes in polysomes.

rRNA G-quadruplex-forming sequences are observed throughout the Chordata phylum.

Translation is universal and highly conserved, presenting special problems and opportunities for phylogenetic analysis. To specifically focus on translation we have developed the SEREB Database[1], which includes all major phyla, yet samples the tree of life in a sparse, efficient and accurate manner. Here we extended the SEREB database from 10 chordate species to 17 for our analysis of ES7 *tentacle a*.

G-quadruplex-forming sequences in chordate ES7s. Our MSA confirms that the lengths of rRNA tentacles of eukaryotes are variable, reaching maxima in species such as *G. gallus* and *H. sapiens*. ES7s of various eukaryotes are illustrated in Figure 5, demonstrating the preferential location of G-quadruplex-forming sequences near the termini of the tentacles. In some species, the number of G-tracts in ES7 is less than four (n<4). G-tracts outside of the motif $G_{\geq 3}N_{1\text{-}7}G_{\geq 3}N_{1\text{-}7}G_{\geq 3}N_{1\text{-}7}G_{\geq 3}$ have also been reported to be capable of forming G-quadruplexes. In addition, it is possible that G-tracts with n<4 form intermolecular G-quadruplexes in polysomes.

G-quadruplex-forming sequences in chordate ESs other than ES7. Our analysis of the extended SEREB Sequence Database suggests that G-quadruplex-forming sequences are universal to chordates (Table S.2). Several chordate species present G-quadruplex-forming sequences in tentacles other than ES7 (Table S.2).

Absence of G-quadruplex sequences in non-chordate rRNAs. To determine the phylogenic distribution of G-quadruplexes in LSU rRNA, we inspected highly curated sequences of 10 chordate and 20 non-chordate eukaryotes from the SEREB database[1]. Thus far we can find no evidence of G-quadruplex-forming sequences in non-chordate eukaryotes.

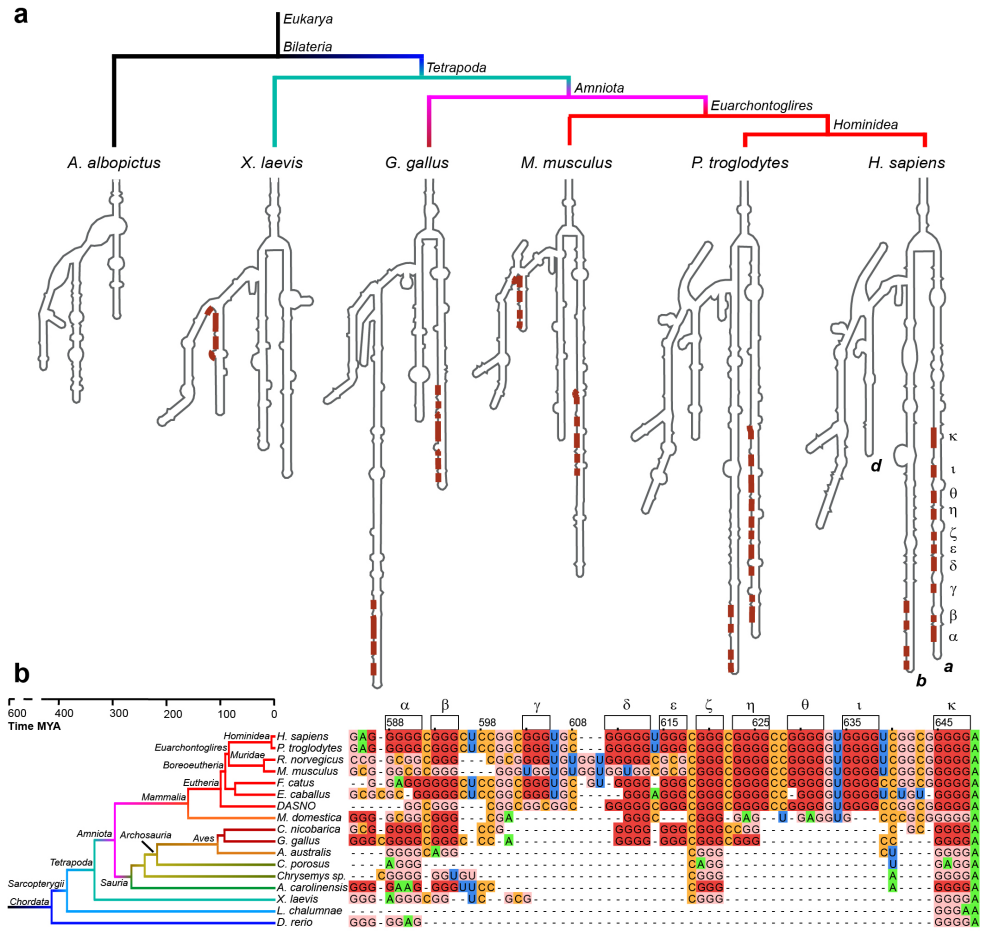

Figure 5. G-tracts in *tentacle a* are observed in birds and mammals. a) Secondary structural models of ES7 from various eukaryotes. G-tracts with $G_{\geq 3}N_{1\text{-}7}G_{\geq 3}N_{1\text{-}7}G_{\geq 3}N_{1\text{-}7}G_{\geq 3}$ are highlighted in red. b) Sequence alignment of *tentacle a* showing conservation of G-quadruplex-forming sequences in chordates. G-tracts in both panels are labeled with Greek symbols. Nucleotides are colored by type. G's within G-tracts are dark red. Other G's are light red. All nucleotides are numbered in accordance with *H. sapiens* 28S rRNA. Sizes of eukaryotic ES7 secondary structures are not to scale. Complete species nomenclature is provided in Table S.3.

RNA remodeling proteins bind selectively to rRNA G-quadruplexes. The localization of rRNA G-quadruplex sequences on ribosomal surfaces suggests they interact with non-ribosomal proteins. To identify the proteins that bind to these G-quadruplexes, we performed pull-down experiments using stable isotope labeling with amino acids in cell culture (SILAC). We focused on GQES7-1, the longest and most stable G-quadruplex-forming region in human rRNA (Figure 6). GQES7-1 rRNA was linked on the 3' end to biotin (GQES7-1-Biotin) and the interacting proteins were pulled down and analyzed by mass spectrometry.

The biotinylation of GQES7-1 did not disrupt the G-quadruplexes (Figure S.5). Several known G-quadruplex-binding proteins were pulled down by this assay (CNBP, YBOX1, hnRP F, hnRP H, DDX21, DDX17)[36-41]. Also, a significant number of helicases were identified (DDX3, CNBP, DDX21, DDX17). All these helicases except DDX3 have been reported to unfold G-quadruplexes[36, 40-41]. In addition, a significant number of heterogeneous nuclear ribonucleoproteins (hnRNPs) were bound to GQES7-1, including hnRNP G-T/RMXL2, hnRNP M, hnRNP G/RBMX, hnRNP H2, hnRNP H, hnRNP F, hnRNP H3, and FUS. hnRNPs are a family of RNA-binding proteins with functions including pre-mRNA processing and transport of mRNAs to ribosomes[42]. Several of these proteins have been previously identified as ribosome-binding proteins[43].

To support results of the pull-down experiments, Western blotting was performed with four of the resulting proteins (Figure 6d). We assayed a DEAD-box RNA helicase (DDX3), a heterogeneous nuclear ribonucleoprotein (hnRNP H), the RNA-binding protein FUS, and a pre-mRNA polyadenylation stimulator (FIP1). hnRNP H is the only member of this group previously identified as a G-quadruplex-binding protein. However, all four proteins are seen to bind to GQES7-1 in the Western blot, suggesting we have tapped an uncharacterized pool of G-quadruplex-binding proteins.

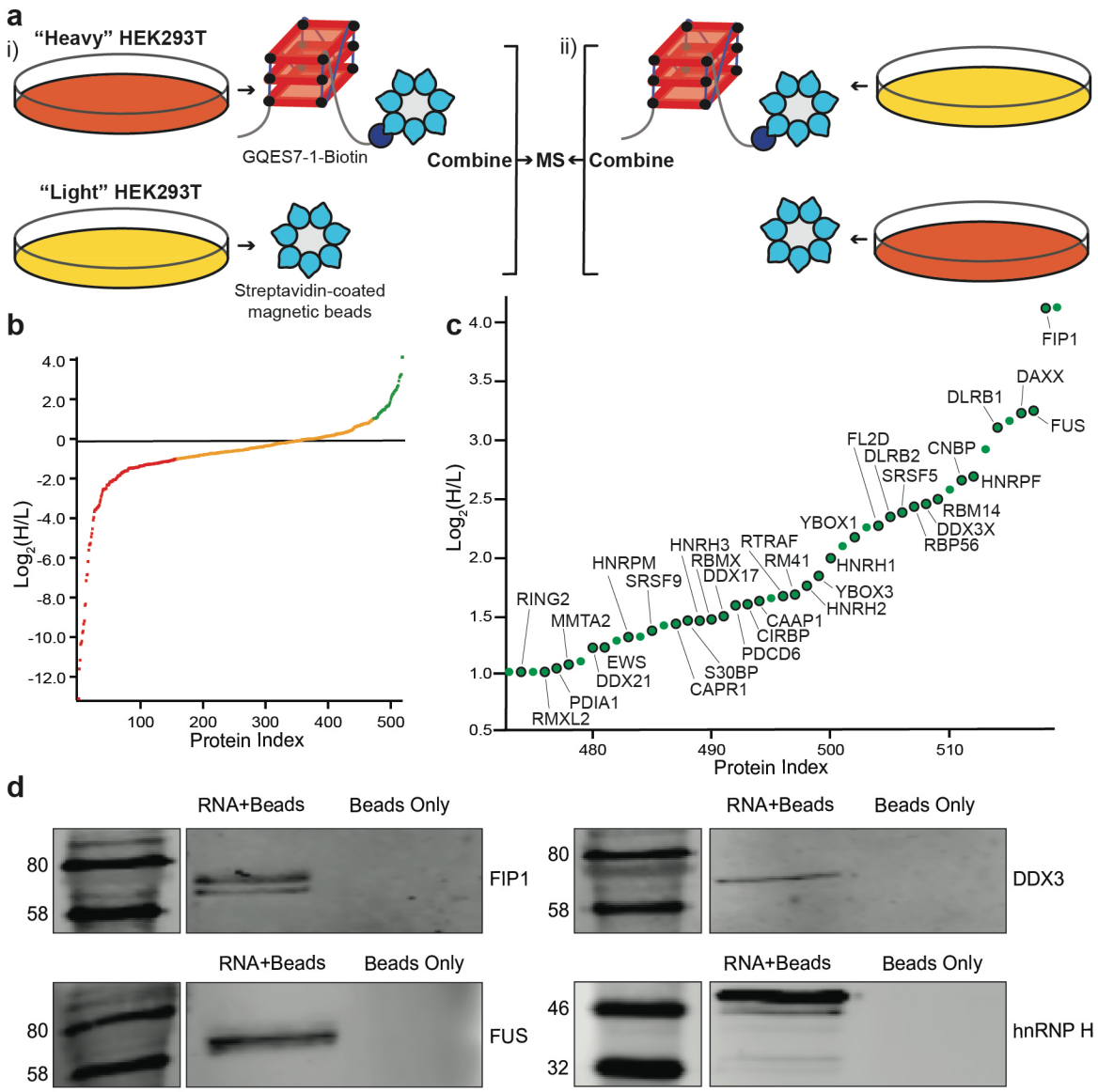

Figure 6. Identification of GQES7-1-binding proteins. a) Scheme of SILAC experiment. "RNA+beads" samples were combined in HEK293T grown in heavy media (i). The "Beads Only" control sample was combined in HEK293T grown in light media. To verify the proteins identified by this method, the experiment was performed using reverse labeling (ii). b) Scatter plot representing fold enrichment of the proteins binding to GQES7-1 in "Heavy" HEK293T. Color representation indicates specific proteins that bound more tightly to GQES7-1 than to the beads (green), to the beads than to GQES7-1 (red) or bound to the beads and GQES7-1 to a similar extent (orange). c) A close-up of the green region of the scatter plot represented in b). Dots with a black contour are used to indicate proteins that appeared in the green region of the two replicate experiments described in a). d) Western blotting analyses of the eluted proteins from the RNA pull-down of HEK293T. All four blotted proteins (FIP1, FUS, DDX3 and hnRNP H) eluted from the GQES7-1 sample (RNA+Beads) but not from the control (Beads Only), confirming the SILAC results.

DISCUSSION

RNA G-quadruplexes have been studied predominantly in the context of mRNAs, where they have been shown to help regulate expression of certain proteins. The results presented in this study indicate that the LSU rRNA, one of the most abundant and ancient RNAs found in nature can contain sequences capable of forming G-quadruplexes (Figure 7). Computation, *in vitro* ThT fluorescence, CD spectroscopy, EMSAs, nuclease digestion and blotting with an anti-G-quadruplex antibody provide a consistent picture of the relative propensities of G-quadruplex formation in the human 28S rRNA. Our phylogenetic analysis suggests that the 28S rRNA of all chordate ribosomes contains G-quadruplex-forming sequences near the termini of specific rRNA tentacles. Our results suggest that nature's most complex organisms have evolved long rRNA tentacles with unexpected polymorphism, including the ability to convert to G-quadruplexes. At the limit, these sequences can be hundreds of Ångströms from the ribosomal core, suggesting roles in recruiting specific proteins or in stabilizing polysomes.

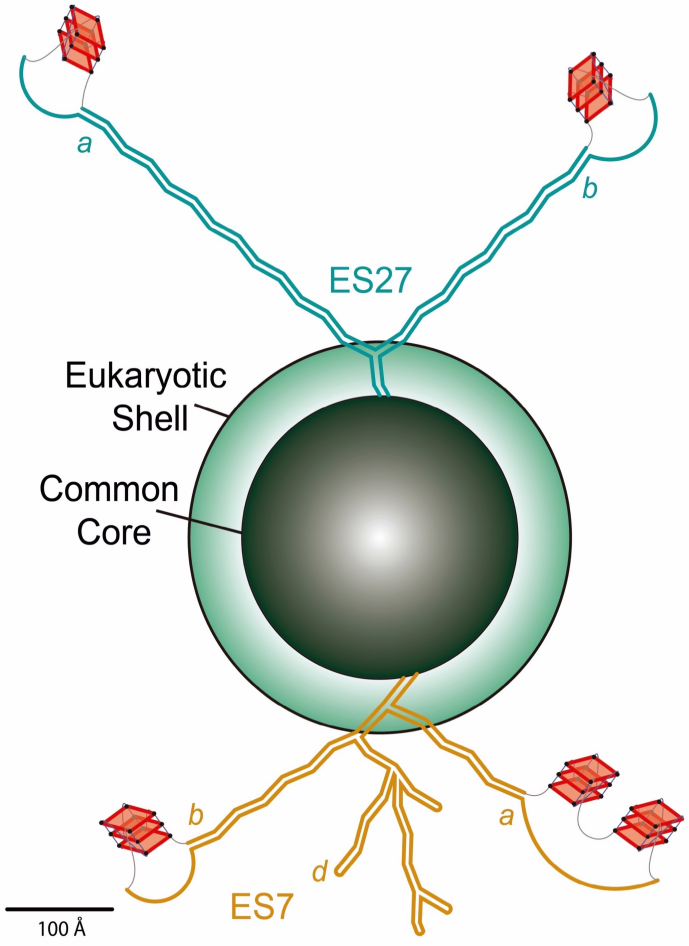

Figure 7. Schematic representation of the common core, the eukaryotic shell and the tentacles of metazoan ribosomes. G-quadruplexes are indicated on the tentacles of ES7 and ES27 in the LSU of the *Homo sapiens* ribosome. The lengths of $ES7_{HS}$ (orange) and $ES27_{HS}$ (green) tentacles are roughly scaled to the size of the common core. *Tentacles a, b,* and *d* ($ES7_{HS}$) and *tentacles a* and *b* ($ES27_{HS}$) are indicated. *Tentacle a* of ES7 is represented as two G-quadruplexes based on our results, which indicate more extensive and/or more stable G-quadruplexes than those found in *tentacle b*. The G-quadruplex region found in Helix 63 of $ES27_{HS}$ is not represented here. The G-quadruplexes represented in *tentacle b* of $ES27_{HS}$ do not fall within the $G_{\geq 3}N_{1\text{-}7}G_{\geq 3}N_{1\text{-}7}G_{\geq 3}N_{1\text{-}7}G_{\geq 3}$ motif but this region contains extensive G-tracts (Table 1) that could potentially form G-quadruplexes.

G-quadruplex-forming rRNA sequences appear to be a general feature of ribosomes of the phylum Chordata. We have inferred this by multiple sequence alignments of representative organisms. The specific sequences and exact locations of the G-quadruplexes on the tentacles are variable in different species. We searched the SEREB database and could find no evidence of G-quadruplex-forming sequences outside of the Chordata phylum. The SEREB database is specifically designed for rRNA analysis, and includes species from all major phyla, and samples the tree of life in a sparse, efficient and accurate manner[1]. It contains complete and highly curated rRNA sequences.

To our knowledge, the possibility that ribosomes are loci of G-quadruplexes has not been investigated previously. G-quadruplex-forming sequences have been described in genes encoding for rRNA, where they are proposed to influence transcription[44] and bind to the nucleolar protein nucleophosmin[45]. However, these studies have focused on the external and internal transcribed regions (ETS and ITS) and are not part of the assembled ribosome. RNA G-quadruplexes have been observed previously in the cytoplasm of human cells[34]. G-quadruplexes are known to bind tightly to a wide variety of proteins.

The extent to which G-quadruplexes form in the context of cellular environments remains uncertain. Bartel and coworkers have suggested that mRNA G-quadruplexes are globally unfolded in eukaryotic cells, presumably by a mechanism involving regulated unwinding factors[46]. These experiments focused on poly-adenylated mRNAs rather than rRNAs, but these unwinding factors may influence G-quadruplexes in rRNA.

The preferential localization of rRNA G-quadruplex region near the termini of specific tentacles of ES7 and ES27 suggests these regions as loci for specific cytosolic proteins. Here we identified multiple human RNA helicases and other RNA remodeling proteins that bind

to rRNA G-quadruplexes. These proteins could be participants in G-quadruplex regulation on ribosomes.

Our observation that polysomes appear to form more extensive G-quadruplexes than monomer ribosomes suggests a role for intermolecular G-quadruplexes in closely associated ribosomes. Our work points to the possibility that, inside cells, ribosomes present polymorphic tentacles that can switch between unimolecular and multimolecular G-quadruplexs and duplex forms. In this model, surfaces of ribosomes contain fluid docking sites for G-quadruplex-specific proteins and foci for nucleic acid assemblies, including in polyribosomes.

The experiments presented in this study were performed in a cell-free environment. The extent to which rRNA G-quadruplexes form inside cells as well as their specific cellular functions remain to be determined. Our work extends the potential functions of rRNA expansion segments, which in chordates are elaborated by G-quadruplex-forming sequences. Their localization on surface-exposed rRNA suggests these structures are important sinks for specific proteins and inter-ribosome interactions.

ACKNOWLEDGEMENTS

The authors thank Dr. Jonathan B. Chaires for helpful discussions and Dr. Lizzette M. Gómez Ramos for designing the negative G-quadruplex controls. Purified 80S ribosomes and polysomes were a gift from Immagina BioTechnology. This work was supported by NASA (NNX16AJ28G and NNX16AJ29G to LDW) and the National Institutes of Health (R01GM118803 to RW).

CONFLICT OF INTEREST

The authors declare that they have no conflict of interest.

AUTHOR CONTRIBUTIONS

SMF, SS, CI, ASP, RMW, RW, and LDW conceived and designed the experiments; SMF, SS and CI performed the experiments; ASP and PIP conducted the phylogenetic analysis. SMF, PIP, SS, ASP, RMW, RW, and LDW analyzed data; SMF, PIP, SS and LDW prepared figures; and SMF, PIP and LDW wrote the paper.

REFERENCES:

1. Bernier, C. R.; Petrov, A. S.; Kovacs, N. A.; Penev, P. I.; Williams, L. D., Translation: The Universal Structural Core of Life. *Mol. Biol. Evol.* **2018,** *34* (9), 2065–2076.
2. Ware, V. C.; Tague, B. W.; Clark, C. G.; Gourse, R. L.; Brand, R. C.; Gerbi, S. A., Sequence analysis of 28S ribosomal DNA from the amphibian *Xenopus laevis*. *Nucleic Acids Res.* **1983,** *11* (22), 7795-817.
3. Clark, C. G.; Tague, B. W.; Ware, V. C.; Gerbi, S. A., *Xenopus laevis* 28S ribosomal RNA: a secondary structure model and its evolutionary and functional implications. *Nucleic Acids Res.* **1984,** *12* (15), 6197-220.
4. Hassouna, N.; Michot, B.; Bachellerie, J. P., The complete nucleotide sequence of mouse 28S rRNA gene. Implications for the process of size increase of the large subunit rRNA in higher eukaryotes. *Nucleic Acids Res.* **1984,** *12* (8), 3563-83.
5. Gerbi, S. A., Expansion segments: Regions of variable size that interrupt the universal core secondary structure of ribosomal RNA. In *Ribosomal RNA—Structure, evolution, processing, and function in protein synthesis*, Zimmermann, R. A.; Dahlberg, A. E., Eds. CRC Press: Boca Raton, FL, 1996; pp 71–87.
6. Ramesh, M.; Woolford, J. L., Jr., Eukaryote-specific rRNA expansion segments function in ribosome biogenesis. *RNA* **2016,** *22* (8), 1153-62.
7. Leidig, C.; Bange, G.; Kopp, J.; Amlacher, S.; Aravind, A.; Wickles, S.; Witte, G.; Hurt, E.; Beckmann, R.; Sinning, I., Structural characterization of a eukaryotic chaperone--the ribosome-associated complex. *Nat. Struct. Mol. Biol* **2013,** *20* (1), 23-8.
8. Gumiero, A.; Conz, C.; Gesé, G. V.; Zhang, Y.; Weyer, F. A.; Lapouge, K.; Kappes, J.; Von Plehwe, U.; Schermann, G.; Fitzke, E., Interaction of the cotranslational Hsp70 Ssb with ribosomal proteins and rRNA depends on its lid domain. *Nat. Commun.* **2016,** *7*, 13563.
9. Melnikov, S.; Ben-Shem, A.; Garreau de Loubresse, N.; Jenner, L.; Yusupova, G.; Yusupov, M., One core, two shells: bacterial and eukaryotic ribosomes. *Nat. Struct. Mol. Biol.* **2012,** *19* (6), 560-7.
10. Lane, A. N.; Chaires, J. B.; Gray, R. D.; Trent, J. O., Stability and kinetics of G-quadruplex structures. *Nucleic Acids Res.* **2008,** *36* (17), 5482-5515.
11. Huppert, J. L.; Bugaut, A.; Kumari, S.; Balasubramanian, S., G-quadruplexes: the beginning and end of UTRs. *Nucleic Acids Res.* **2008,** *36* (19), 6260-6268.
12. Eddy, J.; Maizels, N., Conserved elements with potential to form polymorphic G-quadruplex structures in the first intron of human genes. *Nucleic Acids Res.* **2008,** *36* (4), 1321-1333.
13. del Villar-Guerra, R.; Gray, R. D.; Chaires, J. B., Characterization of quadruplex DNA structure by circular dichroism. *Curr. Protoc. Nucleic Acid Chem.* **2017**, 17.8. 1-17.8. 16.
14. Shcherbakov, D.; Piendl, W., A novel view of gel-shifts: analysis of RNA-protein complexes using a two-color fluorescence dye procedure. *Electrophoresis* **2007,** *28* (5), 749-55.
15. Bernier, C.; Petrov, A. S.; Waterbury, C.; Jett, J.; Li, F.; Freil, L. E.; Xiong, b.; Wang, L.; Le, A.; Milhouse, B. L.; Hershkovitz, E.; Grover, M.; Xue, Y.; Hsiao, C.; Bowman, J. C.; Harvey, S. C.; Wartel, J. Z.; Williams, L. D., RiboVision: Visualization and Analysis of Ribosomes. *Faraday Discuss* **2014,** *169* (1), 195-207.

16. Altschul, S. F.; Madden, T. L.; Schaffer, A. A.; Zhang, J.; Zhang, Z.; Miller, W.; Lipman, D. J., Gapped BLAST and PSI-BLAST: a new generation of protein database search programs. *Nucleic Acids Res.* **1997,** *25* (17), 3389-402.
17. Database Resources of the National Center for Biotechnology Information. *Nucleic Acids Res* **2017,** *45* (D1), D12-d17.
18. Katoh, K.; Standley, D. M., A simple method to control over-alignment in the MAFFT multiple sequence alignment program. *Bioinformatics* **2016,** *32* (13), 1933-1942.
19. Hall, T. A. In *BioEdit: a user-friendly biological sequence alignment editor and analysis program for Windows 95/98/NT*, Nucleic Acids Symp. Ser., [London]: Information Retrieval Ltd., c1979-c2000.: 1999; pp 95-98.
20. Waterhouse, A. M.; Procter, J. B.; Martin, D. M.; Clamp, M.; Barton, G. J., Jalview Version 2—a multiple sequence alignment editor and analysis workbench. *Bioinformatics* **2009,** *25* (9), 1189-1191.
21. Hedges, S. B.; Dudley, J.; Kumar, S., TimeTree: a public knowledge-base of divergence times among organisms. *Bioinformatics* **2006,** *22* (23), 2971-2972.
22. Eng, J. K.; McCormack, A. L.; Yates, J. R., An approach to correlate tandem mass spectral data of peptides with amino acid sequences in a protein database. *Journal of the American Society for Mass Spectrometry* **1994,** *5* (11), 976-989.
23. Kikin, O.; D'Antonio, L.; Bagga, P. S., QGRS Mapper: a web-based server for predicting G-quadruplexes in nucleotide sequences. *Nucleic Acids Res.* **2006,** *34* (Web Server issue), W676-82.
24. Lammich, S.; Kamp, F.; Wagner, J.; Nuscher, B.; Zilow, S.; Ludwig, A.-K.; Willem, M.; Haass, C., Translational repression of the disintegrin and metalloprotease ADAM10 by a stable G-quadruplex secondary structure in its 5′-untranslated region. *J. Biol. Chem.* **2011,** *286* (52), 45063-45072.
25. Xu, S.; Li, Q.; Xiang, J.; Yang, Q.; Sun, H.; Guan, A.; Wang, L.; Liu, Y.; Yu, L.; Shi, Y., Thioflavin T as an efficient fluorescence sensor for selective recognition of RNA G-quadruplexes. *Scientific Reports* **2016,** *6*.
26. Renaud de la Faverie, A.; Guédin, A.; Bedrat, A.; Yatsunyk, L. A.; Mergny, J.-L., Thioflavin T as a fluorescence light-up probe for G4 formation. *Nucleic Acids Res.* **2014,** *42* (8), e65-e65.
27. Zhang, S.; Sun, H.; Chen, H.; Li, Q.; Guan, A.; Wang, L.; Shi, Y.; Xu, S.; Liu, M.; Tang, Y., Direct visualization of nucleolar G-quadruplexes in live cells by using a fluorescent light-up probe. *Biochim Biophys Acta* **2018,** *1862* (5), 1101-1106.
28. von Hacht, A.; Seifert, O.; Menger, M.; Schutze, T.; Arora, A.; Konthur, Z.; Neubauer, P.; Wagner, A.; Weise, C.; Kurreck, J., Identification and characterization of RNA guanine-quadruplex binding proteins. *Nucleic Acids Res.* **2014,** *42* (10), 6630-44.
29. Fratta, P.; Mizielinska, S.; Nicoll, A. J.; Zloh, M.; Fisher, E. M.; Parkinson, G.; Isaacs, A. M., *C9orf72* hexanucleotide repeat associated with amyotrophic lateral sclerosis and frontotemporal dementia forms RNA G-quadruplexes. *Scientific Reports* **2012,** *2*, 1016.
30. Halder, K.; Wieland, M.; Hartig, J. S., Predictable suppression of gene expression by 5'-UTR-based RNA quadruplexes. *Nucleic Acids Res.* **2009,** *37* (20), 6811-7.
31. Arora, A.; Dutkiewicz, M.; Scaria, V.; Hariharan, M.; Maiti, S.; Kurreck, J., Inhibition of translation in living eukaryotic cells by an RNA G-quadruplex motif. *RNA* **2008,** *14* (7), 1290-6.

32. Kumari, S.; Bugaut, A.; Huppert, J. L.; Balasubramanian, S., An RNA G-quadruplex in the 5' UTR of the NRAS proto-oncogene modulates translation. *Nat Chem. Biol.* **2007,** *3* (4), 218-21.
33. Choi, K. H.; Choi, B. S., FORMATION OF A HAIRPIN STRUCTURE BY TELOMERE 3' OVERHANG. *Biochim. Biophys. Acta-Gene Struct. Expression* **1994,** *1217* (3), 341-344.
34. Biffi, G.; Di Antonio, M.; Tannahill, D.; Balasubramanian, S., Visualization and selective chemical targeting of RNA G-quadruplex structures in the cytoplasm of human cells. *Nat. Chem.* **2014,** *6* (1), 75-80.
35. Biffi, G.; Tannahill, D.; McCafferty, J.; Balasubramanian, S., Quantitative visualization of DNA G-quadruplex structures in human cells. *Nat. Chem.* **2013,** *5* (3), 182-6.
36. Benhalevy, D.; Gupta, S. K.; Danan, C. H.; Ghosal, S.; Sun, H.-W.; Kazemier, H. G.; Paeschke, K.; Hafner, M.; Juranek, S. A., The human CCHC-type zinc finger nucleic acid-binding protein binds G-rich elements in target mRNA coding sequences and promotes translation. *Cell reports* **2017,** *18* (12), 2979-2990.
37. Khateb, S.; Weisman-Shomer, P.; Hershco-Shani, I.; Ludwig, A. L.; Fry, M., The tetraplex (CGG) n destabilizing proteins hnRNP A2 and CBF-A enhance the in vivo translation of fragile X premutation mRNA. *Nucleic Acids Res.* **2007,** *35* (17), 5775-5788.
38. Matunis, M. J.; Xing, J.; Dreyfuss, G., The hnRNP F protein: unique primary structure, nucleic acid-binding properties, and subcellular localization. *Nucleic Acids Res.* **1994,** *22* (6), 1059-1067.
39. Caputi, M.; Zahler, A. M., Determination of the RNA binding specificity of the heterogeneous nuclear ribonucleoprotein (hnRNP) H/H′/F/2H9 family. *J. Biol. Chem.* **2001,** *276* (47), 43850-43859.
40. McRae, E. K.; Booy, E. P.; Padilla-Meier, G. P.; McKenna, S. A., On Characterizing the Interactions between Proteins and Guanine Quadruplex Structures of Nucleic Acids. *Journal of nucleic acids* **2017,** *2017*.
41. Dardenne, E.; Espinoza, M. P.; Fattet, L.; Germann, S.; Lambert, M.-P.; Neil, H.; Zonta, E.; Mortada, H.; Gratadou, L.; Deygas, M., RNA helicases DDX5 and DDX17 dynamically orchestrate transcription, miRNA, and splicing programs in cell differentiation. *Cell reports* **2014,** *7* (6), 1900-1913.
42. Chaudhury, A.; Chander, P.; Howe, P. H., Heterogeneous nuclear ribonucleoproteins (hnRNPs) in cellular processes: Focus on hnRNP E1's multifunctional regulatory roles. *RNA* **2010**.
43. Simsek, D.; Tiu, G. C.; Flynn, R. A.; Byeon, G. W.; Leppek, K.; Xu, A. F.; Chang, H. Y.; Barna, M., The mammalian ribo-interactome reveals ribosome functional diversity and heterogeneity. *Cell* **2017,** *169* (6), 1051-1065. e18.
44. Drygin, D.; Siddiqui-Jain, A.; O'Brien, S.; Schwaebe, M.; Lin, A.; Bliesath, J.; Ho, C. B.; Proffitt, C.; Trent, K.; Whitten, J. P., Anticancer activity of CX-3543: a direct inhibitor of rRNA biogenesis. *Cancer Res.* **2009,** *69* (19), 7653-7661.
45. Chiarella, S.; De Cola, A.; Scaglione, G. L.; Carletti, E.; Graziano, V.; Barcaroli, D.; Lo Sterzo, C.; Di Matteo, A.; Di Ilio, C.; Falini, B., Nucleophosmin mutations alter its nucleolar localization by impairing G-quadruplex binding at ribosomal DNA. *Nucleic Acids Res.* **2013,** *41* (5), 3228-3239.
46. Guo, J. U.; Bartel, D. P., RNA G-quadruplexes are globally unfolded in eukaryotic cells and depleted in bacteria. *Science* **2016,** *353* (6306), aaf5371.